NEANDC (E) 225 "L"
INDC (FR) 52/L

# FAST NEUTRON CAPTURE ACTIVITIES AT BRUYERES-LE-CHATEL

by

S. JOLY

*Service de Physique Neutronique et Nucléaire*
*Centre d'Etudes de Bruyères-le-Châtel*
*B.P. N° 561*
*92542 MONTROUGE CEDEX, France*

JUILLET 1981

COMMISSARIAT A L'ENERGIE ATOMIQUE
FRANCE

RAPPORT NEANDC-INDC - Serge JOLY

ETUDE DE LA CAPTURE RADIATIVE DE NEUTRONS RAPIDES A BRUYERES-LE-CHATEL

Sommaire.- Dans ce rapport sont résumées les études sur la réaction de capture radiative de neutrons rapides. Les différentes manières de déduire la section efficace totale de capture à partir du spectre d'amplitude délivré par un détecteur NaI sont présentées. L'étude des probabilités d'émission gamma et des mécanismes de la réaction de capture est faite pour des neutrons d'énergie comprise entre 0,5 et 6 MeV.

1981 31 p.

Commissariat à l'Energie Atomique - France

---

RAPPORT NEANDC-INDC - Serge JOLY

FAST NEUTRON CAPTURE ACTIVITIES AT BRUYERES-le-CHATEL

Summary.- Fast neutron capture activities at Bruyères-le-Châtel are summarized. The different ways of deducing total capture cross sections from the pulse-height distributions as given by a NaI detector are described. The distribution of radiative strength in nuclei is deduced and the radiative neutron capture mechanisms are investigated for neutron energies between 0.5 and 5.0 MeV.

1981 31 p.

Commissariat à l'Energie Atomique - France

NEANDC (E) 225 "L"
INDC (FR) 52/L

# FAST NEUTRON CAPTURE ACTIVITIES AT BRUYERES-LE-CHATEL

by

S. JOLY

*Service de Physique Neutronique et Nucléaire*
*Centre d'Etudes de Bruyères-le-Châtel*
*B.P. N° 561*
*92542 MONTROUGE CEDEX, France*

JUILLET 1981

COMMISSARIAT A L'ENERGIE ATOMIQUE
FRANCE

CONTENTS

## I - INTRODUCTION

In this paper, we report on the fast neutron capture activities under way at Bruyères-le-Châtel. We first present the experimental procedure and the data analysis technique developed to investigate the neutron capture reaction in the energy range from 0.5 to 6.0 MeV. Total capture cross sections are determined by means of the integrated spectrum technique using the capture spectrum shape. This method provides also the possibility of deducing the $\gamma$-ray strength function for compound nuclei formed in the $(n,\gamma)$ reaction. The $^{89}Y(n,\gamma_0 + \gamma_1)$ and $^{208}Pb(n,\gamma_0)$ cross sections have been measured between 0.5 and 6.0 MeV to investigate the relative contribution of the compound-nucleus and direct-semi-direct (DSD) processes in this energy range. Asymmetry factor has been measured for the $\gamma_0$-transition to the ground-state in $^{209}Pb$ and compared to the predictions of the DSD model when the excitation of the M1 resonance is taken into account. Finally, we mention recent experiments performed at Los Alamos where the effect of the isovector quadrupole resonance on the asymmetry factor was studied for the $^{208}Pb(n,\gamma_0)$ reaction in the energy range $E_n$ = 16 to 20 MeV.

## II - EXPERIMENTAL AND DATA PROCESSING TECHNIQUES

The experimental set-up used for our fast neutron capture activities[1] is shown schematically in fig.1. Depending on the desired neutron energy, the $^7Li(p,n)^7Be$ ($E_n \leq 0.7$ MeV), $^3H(p,n)^3He$ and $^2H(d,n)^3He$ ($E_n > 3.5$ MeV) reactions are used as sources of monoenergetic neutrons of variable energy. A pulsed and bunched proton (deuteron) beam is delivered by the 4 MV Van de Graaff generator at Bruyères-le-Châtel. The pulse width is about 1 ns and the average particle beam intensity between 4 and 10 µA. The time-of-flight technique is used to reduce the background due to scattered neutrons and to separate capture $\gamma$-rays of interest from those due to other sources, thus improving the signal-to-background ratio. The targets consist of metallic lithium or tritium adsorbed in titanium on tantalum backings. The deuterium gas is contained in a cylindrical cell 1.5 cm long at pressures between 1.0 and 2.0 atm.

Generally, samples are disks 60 mm in diameter and thicknesses between 1 and 6 mm. The thickness is a compromise between counting rate, on one hand, and neutron multiple scattering, gamma-ray and neutron attenuation effects, on the other hand. We have also used samples with a cylinder shape. Samples are located at 8 cm from the target centre.

Gamma-rays are detected by a 76 mm diameter by 152 mm long NaI crystal surrounded by a NaI annulus. This spectrometer is used in the anti-Compton and first-escape modes simultaneously. The γ-ray detector efficiency, as a function of γ-ray energy between 1.0 and 12.5 MeV, is determined by calibrated radioactive sources and by nuclear reactions. The same sources and reactions were used to build the response matrices of the spectrometer.

The spectrometer is placed in the centre of a large shield constructed of special neutron and γ-ray absorbing materials. The distance between the detector and the sample is typically 80 cm and with such a small detection solid angle, the energy distribution of the γ-rays can be obtained. The 50 mm diameter collimator aperture contains a 200 mm long $^{6}$LiH cylinder for attenuation of the neutrons scattered by the sample. A tungsten and lead shadow bar is added to shield the gamma-ray detector from direct target radiation. The effectiveness of our shielding system is reflected by a very low and flat time-of-flight spectrum when running without sample.

The neutron flux is measured by a calibrated long counter[2]) located at 0° compared to the beam direction and at about 2 m from the neutron source.

The net pulse-height spectra are converted to gamma-ray distributions using a least-squares unfolding method and the response functions of the spectrometer. Finally, the unfolded spectra are corrected for γ-ray efficiency of the spectrometer and for γ-ray attenuation in the sample in order to give the capture γ-ray spectrum emitted by the sample. This is done for the two detection modes and we use the weighted average of the two energy distributions. The accurate knowledge of the γ-ray spectrum is of vital importance for our method of deducing capture cross sections (and to determine γ-ray strength functions as we shall see later) so special efforts have been devoted to get the spectrum shape with a good accuracy.

The neutron flux, as determined by the long counter, is corrected for the anisotropy of the neutron source , for the transmission of neutrons through the sample and through the air between the sample and the monitor. The γ-ray yield recorded by the detector is also corrected for the neutron flux variation in the sample which is a combined effect of neutron attenuation and multiple scattering. Except for multiple scattering, these corrections have been estimated using analytical expressions[3]) and a modified Monte-Carlo[4]) code. The

results were found to be in very good agreement as quoted in table 1 for the $^{208}Pb(n,\gamma_o)$ reaction. The neutron multiple scattering effect was estimated using the Monte-carlo technique.

## III - CAPTURE CROSS SECTIONS

Capture and inelastic gamma-rays following the interaction of neutrons with the sample are detected by the NaI crystal. Unfortunately, for the neutron energies we are interested in ($0.5 \leq E_n \leq 3.0$ MeV), the contribution of the $\gamma$-rays from the $(n,n'\gamma)$ reaction is very important in the low-energy part ($E_\gamma < E_n$) of the measured distribution. It is not then possible to use this low-energy region and we have to estimate the capture contribution in this region. For low-energy neutrons ($E_n \leq 1.0$ MeV), the energy region where the spectrum contains only capture events is also limited by the lower discriminator level ( $\sim$ 1.0 MeV). The method we developed combines the technique used to study gamma-ray strength functions and the spectrum method of measuring partial neutron cross sections[1]).

In fact, two methods were considered to determine capture cross sections from the capture spectra.

In the first method (method I), the unknown part of the capture spectrum is deduced by means of the statistical model. The shape of the capture spectrum is determined by the energy dependence of the $\gamma$-ray strength function $f(E_\gamma)$ and by the level-density distribution $\rho(U)$. This level-density distribution has to be determined from other sources and the $f(E_\gamma)$ function is obtained by the best fit between the observed and computed $\gamma$-ray distributions in the energy region containing only capture events ($E_\gamma > E_n$). The strength function is extrapolated down to $E_\gamma = 0$ to obtain the entire capture spectrum. The extrapolation of the capture spectrum is thus replaced by the extrapolation of the $f(E_\gamma)$ function. The level-density distribution is not critical for this cross section purpose because a different distribution would give an other energy dependence for $f(E_\gamma)$ in the region of the fit (the measured capture spectrum shape remaining the same) and a different extrapolation to zero. This effect introduces a small additional uncertainty on the cross sections. The number of capture reactions $R_c$ is then given by the ratio between the observed $\gamma$-ray spectrum $S(E_\gamma)$ and the computed spectrum per capture $\nu(E_\gamma)$ :

$$R_c = \int_{E_{min}}^{U_{max}} S(E_\gamma)\, dE_\gamma \Big/ \int_{E_{min}}^{U_{max}} \nu(E_\gamma) dE_\gamma \qquad (1)$$

with $U_{max} = E_n + B_n$ where $B_n$ is the neutron separation energy and $E_{min} \# E_n$. Combined with the neutron fluence and the number N of nuclei in the sample, the capture cross section is given by :

$$\sigma_{n\gamma} = 4\pi \left( \frac{d\sigma}{d\Omega} \right)_{90°} = 4\pi \frac{R_c}{N\emptyset} \qquad (2)$$

We have assumed isotropy for the emitted radiations and the obtained capture cross section is really an angle-integrated cross section. Simple calculations of the angular distribution of primary capture γ-rays in the $^{197}Au(n,\gamma)$ reaction indicated very small anisotropy. This is expected from statistical considerations for neutron energies lower than 4 MeV, or so. When comparison is possible, we found a good agreement between our results and previous data in the 0.5 to 3.0 MeV energy range[5,6]. As an example fig.2 represents the neutron capture cross section for gold which has become a standard.

In the second method (method II), the number of captures $R_c'$ is given by the principle of energy conservation :

$$R_c' = \frac{1}{U_{max}} \int_0^{U_{max}} E_\gamma \, S(E_\gamma) \, dE_\gamma \qquad (3)$$

The observed spectrum $S(E_\gamma)$ has to be extrapolated from $E_\gamma \gtrsim E_n$ down to zero energy. For this extrapolation, two approaches are considered. In the first one, the spectrum shape is assumed to have the following energy dependence :

$$S(E_\gamma) \, dE_\gamma \sim \exp(-\alpha E_\gamma) \, dE_\gamma \qquad (4)$$

where α is a constant. Sometimes the γ-ray spectrum deviates considerably from this behaviour (bumps in gold spectra) and this extrapolation is very uncertain. In the second approach, we assume a constant value of the spectrum distribution $S(E_\gamma) = S(E_{min})$ for $E_\gamma \lesssim E_{min}$. It was observed that the results obtained using method I were between the two values deduced with method II.

Recently, we have investigated the feasibility of the weighting technique to determine capture cross sections when applied to NaI pulse-height spectra[7]. In principle, the pulse-height weighting technique could be applied to any kind of gamma-ray detector to measure neutron capture cross sections.

We can generate an average response function proportional to the energy and when applied to the measured pulse-height spectrum, the area of the weighted spectrum is proportional to the detected γ-ray energy. Dividing this total energy by the total excitation energy in the compound nucleus gives the total number of capture reactions.

From the response functions and the efficiency of our spectrometer, we have deduced the weighting function presented in fig.3. The average total energy emitted by the sample is given by :

$$E_t = \int_0^{U_{max}} E_\gamma \, S(E_\gamma) \, dE_\gamma \qquad (5)$$

By definition of the weighting function W(I) this energy is equal to the total energy contained in the weighted spectrum. Before getting the number of capture reactions by the pulse-height weighting technique, we have to calculate the energy loss in the sample, and add it to the measured total energy.

Using this technique we have determined the capture cross section of $^{181}$Ta at 0.5 and 3.0 MeV. The pulse-height distribution is extrapolated down to zero using three different extrapolations : constant, linear and exponential. The weighted pulse-height spectrum for 3.0 MeV neutrons is presented in fig.4 along with the weighted extrapolations. For this extrapolation purpose, the extrapolation of the pulse-height spectrum is preferred to the extrapolation of the weighted spectrum for it is easier to use the smooth energy dependence of the pulse-height spectrum for $E_\gamma > E_n$. The cross sections deduced from the pulse-height technique are given in table 2 depending on the extrapolations. At 0.5 MeV, the different extrapolations have a little effect on the deduced cross sections. However, at 3.0 MeV this difference is very large because the extrapolated part of the total capture pulse-height spectrum is very important and consequently the deduced cross section is very uncertain.

For the purpose of comparison, these cross sections have also been determined using the spectrum integrated technique; the results are also reported in table 2. At 0.5 MeV, the cross sections obtained using the two techniques are in good agreement. The overall agreement is not as good at 3.0 MeV, the critical problem being the extrapolation influence on the deduced cross section.

In conclusion, the pulse-height weighting technique is found to give very similar results to those obtained with methods I and II as described previously eventhough the extrapolations do not concern the same spectra. This

agreement is quite good as far as the extrapolation energy range is not too important ; $E_n \sim 1.5$ MeV could be the highest energy for using this technique. For neutron energies above 1.0 MeV, method I seems to be the best one because the capture spectrum can be calculated in the low-energy region. However, because of the low capture cross sections in this region, statistics is becoming poor and it is difficult to get cross sections with accuracy better than 20 %.

## IV - GAMMA-RAY STRENGTH FUNCTIONS

The $\gamma$-ray strength function is defined as the distribution, as a function of $\gamma$-ray energy, of the average reduced radiative width for a particular multipole type.

Gamma-ray strength functions are used in the calculation of cross sections and $\gamma$-ray spectra from capture of fast neutrons. In this respect, we have pursued our systematics of $\gamma$-ray strength functions for nuclei in the mass range from A = 90 to A = 210. We have also studied non-statistical effects (bumps) in neutron $\gamma$-ray spectra especially in the regions where the s and p-wave neutron strength functions are at a maximum.

In the present work, we have deduced $\gamma$-ray strength functions by means of the spectrum fitting technique. In this technique, the strength function is obtained calculating the shape and the magnitude of the total $\gamma$-ray spectrum with trial functions until good agreement is achieved with the observed spectrum. Details of the calculation of the total capture spectrum are given in ref.8. Gamma-ray strength functions are determined between 1.5 MeV and the maximum energy, which is an advantage of this technique. However, no information can be obtained in the low-energy region ($E_\gamma < 1.5$ MeV) because of the major contribution from inelastic scattering. The spectrum fitting method is not able to distinguish multipolarities of $\gamma$-rays, and the strength function is a mixture of E1 and M1 strength functions. The main drawback of this technique is the dependence of the deduced strength function on the level-density distribution which has to be obtained from other sources. The level-density distribution is of the form :

$$\rho(U,J) = \rho_o(U)\ (2J+1)\ \exp\ [-J(J+1)/2\sigma^2] \qquad (6)$$

where the spin cut-off factor $\sigma$ is assumed to be energy independent. For the energy dependent part of this distribution, we use ;

$$\rho_o(U) = A \exp(U/T) \tag{7}$$

The parameters A and T are determined from the cumulative number of low-lying excited states and the s-wave neutron spacing at the neutron binding energy. To avoid missing levels, we consider only states populated by thermal neutron radiative capture, i.e., those being reached by dipole transitions from capturing states[8]). However, the spin cut-off factor $\sigma$ is generally not known and we assume that the moment of inertia of the nucleus has a value between 50 % and 100 % of the rigid-body value. The parameters A and T have been deduced for these two extreme values. Uncertainty in the level density introduces the largest uncertainty in the strength functions, the other contribution comes from the statistical accuracy in the pulse-height spectra.

We have determined $\gamma$-ray strength functions for about twenty nuclei in the mass range from A = 90 to A = 206. As examples, we present the results for $^{198}$Au and $^{182}$Ta. The $^{198}$Au $\gamma$-ray strength function is presented in fig.5 for the two parameters T = 0.71 MeV and T = 0 74 MeV. This strength function is compared with photonuclear data as given by the photonuclear absorption cross section $\sigma_{\gamma a}(E_\gamma)$ :

$$f(E_\gamma) = 8.67 \times 10^{-8} \frac{\sigma_{\gamma a}(\text{mb})}{E_\gamma} \ (\text{MeV}^{-3}) \tag{8}$$

The curve (GDR) obtained using the giant dipole resonance parameters is in disagreement with the data below 12 MeV. A better fit is obtained using a Lorentzian shape multiplied by a depression factor; the corresponding strength function is in good agreement with our results. The $f(E_\gamma)$ function can also be obtained from primary $\gamma$-ray transitions averaged over many resonances. This has been done for $4.9 < E_\gamma < 6.4$ MeV as shown in fig.5. The agreement between the extrapolation of the photonuclear data, the average reduced widths of high-energy primary transitions and our results is quite good. In fig.6, we compare the $\gamma$-ray strength function for $^{182}$Ta as deduced by the spectrum fitting technique with the parameters T = 0.55 and T = 0.57 MeV and the $\gamma$-ray strength function obtained from the photoabsorption cross section. There is good agree-

ment between the results.

From our systematics we conclude that the distribution of radiative strength in nuclei is in good agreement with the extrapolation of the giant dipole resonance for most elements far from closed shells. This energy dependence is more realistic than the strength function independent of $E_\gamma$ for dipole transitions as predicted by the single-particle model. We have observed significant clustering of radiative strength around the unperturbed particle-hole energy for several nuclei and are considering modern microscopic theories to explain these effects.

## V - CAPTURE MECHANISM BETWEEN 0.5 AND 6.0 MeV.

Capture cross sections for heavy nuclei are well reproduced by compound-nucleus (CN) calculations for neutron energies below 4.0 MeV. On the other hand, the direct semi-direct (DSD) model[9]) has been found to describe fairly well the general features of the experimental capture results in the giant dipole resonance region. In the intermediate region between 4 and 7 MeV, the CN and DSD contributions are of the same magnitude and are of interest for the study of the interference between these two processes[10]). We report here on the results obtained for the $^{89}Y(n,\gamma_o + \gamma_1)$ and $^{208}Pb(n,\gamma_o)$ reactions.

The $^{89}Y(n,\gamma_o + \gamma_1)$ cross section has been measured in collaboration with Nilsson and coworkers in Uppsala[11]). Measurements have been performed at Bruyères-le-Châtel at neutron energies between 0.5 and 3.0 MeV. The sample was a cylinder 48 mm in diameter and 16 mm in thickness made of elemental yttrium. Because of the 202 keV difference between the $\gamma_o$ and $\gamma_1$ transitions, these could not be separated with a NaI crystal and were considered together in the theoretical calculations as well. The cross sections obtained for the capture to the 2 $d_{5/2}$ ground-state doublet in $^{90}Y$ are presented in fig.7 and compared with previous data[12]). The theoretical excitation functions are also presented in fig.7. Below 4 MeV, the cross sections are in agreement with predictions of the CN model. The DSD model provides a good description of the observed data for neutron energies above 7 MeV.

The $^{208}Pb(n,\gamma_o)$ cross section was measured from 0.8 to 5.9 MeV. The lead sample, enriched at 98.7 % in $^{208}Pb$, was a cylinder 3.9 cm in height and 3.5 cm in diameter with its vertical axis at 8.3 cm from the target axis. The angle-integrated capture cross sections for the $\gamma$-ray transition to the g 9/2

ground-state level of $^{209}Pb$ are presented in fig.8 and compared with previous data[13]) in the GDR region. Around 6.0 MeV the agreement between the two sets of data is quite good. Compound-nucleus calculations for this reaction are in progress. The data obtained at these energies would help in comparing the results from the pure-resonance model (PRM) to the GDR region data[14]).

## VI - INVESTIGATION OF GIANT RESONANCES THROUGH THE DSD MODEL

In the DSD model the reaction amplitude for a given multipolarity is interpreted as the sum of the direct and semidirect (or collective) processes. The transition amplitude for capture of the incident neutron from the continuum optical-model state $|\chi_E^+>$ to the single-particle state $|\psi_{n\ell j}>$ can be written in the form :

$$T = <\psi_{n\ell j} | M | \chi_E^+> + <\psi_{n\ell j} | \frac{V_M}{E_\gamma - E_R + \frac{1}{2} i \Gamma_R} | \chi_E^+> \qquad (9)$$

where M represents the single-particle multipole operator and $V_M$ the form factor for the excitation of the giant resonance, with excitation energy $E_R$ and width $\Gamma_R$. In the first calculations of the model, only the giant dipole resonance was considered. A complex coupling interaction function[15]) having a real part of volume form and a surface peaked imaginary part was able to describe the fast neutron capture data (cross sections and capture spectrum) reasonably well.

Experimental evidence has been accumulated for the isovector and isoscalar E2 resonances and the contributions of these resonances in the radiative capture of nucleons was investigated[16,17]) in addition to the GDR.

More recently, the model was extended including capture proceeding through collective M1 excitation[18]) besides the collective E1 and E2 excitation modes of the target. It was shown[19]) that M1 excitation produces effects on the angular distribution symmetry of the capture $\gamma$-rays. This effect is due to the interference between radiations of different multipolarities. Cross sections for M1 and isoscalar E2 processes are so small compared to the E1 strength that these resonances cannot be investigated directly by means of their cross section even at their maximum.

Generally, the angular distribution of capture γ-rays is presented in the following form :

$$\frac{d\sigma}{d\Omega} = A_o \left[ 1 + \sum_i a_i P_i(\cos \theta_\gamma) \right] \qquad (10)$$

However, determination of the $a_i$ coefficients with a good accuracy is very difficult for (n,γ) reactions and the for-aft asymmetry is preferred :

$$R = \frac{Y(55°) - Y(125°)}{Y(55°) + Y(125°)} \qquad (11)$$

where the yield Y, for the γ-transition of interest, is measured at 55° and 125° with respect to the incident neutron beam. Assuming $a_4$ to be very small, R can be expressed in terms of the Legendre coefficients :

$$R = 0.5736\ a_1 - 0.3886\ a_3 \qquad (12)$$

the $a_1$ coefficient, generated by the M1 and E2 radiations interfering with the dominant E1 radiation, reflects the presence of a collective excitation. In fig.9 we have represented the energy dependence of the R factor for three different excitations of the target nucleus in the $^{208}Pb(n,\gamma_o)$ reaction[19,20]. The negative peak at 3.8 MeV is completely generated by the E1-M1 interference.

We measured the asymmetry factor R at 3.8 and 5.9 MeV to compare it with the predictions of the DSD model when the M1 resonance is considered. The 2.615 MeV γ-ray from the $^{208}Pb(n,n'\gamma)$ reaction was also recorded. The intensities obtained at 55° and 125° were corrected for gamma and neutron attenuation within the sample and for neutron source anisotropy and neutron multipole scattering. After correction, the 2.615 MeV γ-ray intensities were found to be equal within 2.5 % as expected. The measured asymmetry factor R is compared to the calculated factor in fig.9. The results would indicate that the M1 resonance is excited in the $^{208}Pb(n,\gamma_o)$ reaction.

Similar measurements have been made for the $^{140}Ce(n,\gamma_o)$ reaction and the analysis of the data is in progress.

Recently, we investigated the E2 isovector giant resonance through the capture of fast neutrons in the $^{208}Pb\ (n,\gamma_o)$ reaction. These measurements have been done at Los Alamos in collaboration with Drake and coworkers. This

resonance is located around 22.5 MeV and has a width of 5 MeV and we measured the asymmetry factor for the $\gamma_0$- transition in the neutron energy range from 16 to 20 MeV. Preliminary results are presented in Fig. 10 and compared with the DSD predictions [21]. The large asymmetries found for the highest neutron energies would indicate the presence of the isovector GQR.

## VII - CONCLUSION

We were able to measure total capture cross sections in a region where usual techniques are normally difficult to apply ; activation technique and the prompt $\gamma$-ray method using large liquid scintillators, Moxon-Rae or Maier-Leibnitz detectors. Apart from the possibility of measuring cross sections for neutron energies above 0.5 MeV,our technique has the advantage of giving information about the energy distribution of capture $\gamma$-rays.

We would like to point out the difficulties of measuring neutron capture cross sections in the energy range from 0.5 to about 6.0 MeV. As the neutron energy increases the neutron capture cross section decreases to a minimum around 5.0 MeV. Because of the low neutron producing reaction cross sections the neutron flux is not very important, especially for the D(d,n) reaction at $E_d \simeq 1.0$ MeV. Finally, for nuclei with low neutron separation energies, the 6.8 MeV $\gamma$-ray from activation in iodine introduces a further difficulty in extracting capture $\gamma$-ray intensities eventhough the use of an anti-Compton spectrometer helps somewhat.

Using the same experimental set-up and data analysis techniques, we have also investigated different aspects of the radiative neutron capture process :

- compound nucleus, direct-semidirect and interference between these two mechanisms.
- excitation of giant resonances, other than the well known giant dipole resonance.
- distribution of radiative strength.

## REFERENCES


[1]) - S. JOLY, J. VOIGNIER, G. GRENIER, D.M. DRAKE and L. NILSSON, *Nucl. Instr. Meth. 153 (1978) 493.*

[2]) - J.L. LEROY, J.L. HUET and J. GENTIL, *Nucl. Instr. Meth. 88 (1970) 1.*

[3]) - A. LINDHOLM, *private communication.*

[4]) - D.L. SMITH, *Argonne National Laboratory, Report ANL/NDM-17 (1975).*

[5]) - S. JOLY, J. VOIGNIER, G. GRENIER, D.M. DRAKE and L. NILSSON, *Nucl. Sci. Eng. 70 (1979) 53.*

[6]) - J. VOIGNIER, S. JOLY and G. GRENIER, *CEA-Report (1980).*

[7]) - S. JOLY, *to be published in Nucl. Sci. Eng.*

[8]) - S. JOLY, D.M. DRAKE and L. NILSSON, *Phys. Rev.C20 (1979) 2072.*

[9]) - C.F. CLEMENT, A.M. LANE and J.R. ROOK, *Nucl. Phys. 66 (1965) 273; 293.*

[10]) - G. MANTZOURANIS, *Z. Phys. 264 (1973) 405.*

[11]) - A. LINDHOLM, L. NILSSON, M. AHMAD, M. ANWAR, I. BERGQVIST and S. JOLY, *Nucl. Phys. A339 (1980) 205.*

[12]) - I. BERGQVIST, B. PALSSON, L. NILSSON, A. LINDHOLM, D.M. DRAKE, E. ARTHUR, D.K. McDANIELS and P. VARGHESE, *Nucl. Phys. A295 (1978) 256.*

[13]) - I. BERGQVIST, D.M. DRAKE and D.K. McDANIELS, *Nucl. Phys. A191 (1972) 641.*

[14]) - F.S. DIETRICH, and A.K. KERMAN, *Phys. Rev. Lett. 43 (1979) 114.*

[15]) - M. POTOKAR, *Phys. Lett. 46B (1973) 346.*

[16]) - G. LONGO and F. SAPORETTI, *Phys. Lett.* *65B* *(1976) 15.*

[17]) - A. LIKAR and R. MARTINCIC, *Nucl. Phys.* *A350* *(1980) 74.*

[18]) - F. SAPORETTI and R. GUIDOTTI, *Lettere al Nuovo Cimento* *22* *(1978) 202.*

[19]) - F. SAPORETTI and R. GUIDOTTI, *Nucl. Phys.* *A311* *(1978) 284.*

[20]) - F. SAPORETTI and R. GUIDOTTI, *Phys. Lett.* *102B* *(1981) 81.*

[21]) - G. LONGO and F. SAPORETTI, *Nuovo Cimento* *46* *(1978) 509.*

*TABLE I*

*Correction factors for $^{208}Pb(n,\gamma_0)$ at $E_n$ = 5.9 MeV*

| | Analytical expression Ref.3 | Monte Carlo Technique Ref. 4 |
|---|---|---|
| $A_\gamma$ | 1.971 | 1.949 |
| $A_n$ | 1.302 | 1.318 |
| $A_s$ | 1.164 | 1.149 |
| $\pi A$ | 2.987 | 2.952 |

$A_\gamma$ : $\gamma$-ray attenuation in the sample.

$A_n$ : neutron attenuation in the sample.

$A_s$ : neutron source anisctropy.

*TABLE II*

*Neutron capture cross sections of* $^{181}Ta$* *at 0.5 and 3.0 MeV. Comparison between the pulse-height weighting (PHW) and integrated spectrum (IS) techniques.*

| Method | Extrapolation | $\sigma_{n\gamma}$ (mb) $E_n$ = 0.5 MeV | $E_n$ = 3.0 MeV |
|---|---|---|---|
| PHW | Constant | 119 | 17 |
| | Linear | 127 | 22 |
| | Exponential | 132 | 32 |
| IS | Distribution ratio (Method I) | 128 | 20 |
| | Constant (Method II) | 127 | 18 |
| | Exponential | 131 | 23 |

* These cross sections are not corrected for neutron self-shielding and multiple scattering in the sample and for the neutron source anisotropy.

## FIGURE CAPTIONS

Fig.1 - Experimental arrangement used to record capture γ-ray spectra.

Fig.2 - Neutron capture cross section for $^{197}Au(n,\gamma)^{198}Au$.

Fig.3 - Weighting function of the NaI spectrometer.

Fig.4 - Weighted pulse-height spectrum of 3.0 MeV neutron capture in $^{181}Ta$.

Fig.5 - The $^{198}Au$ strength function deduced from the present work is represented by the hatched region. Filled circles are photonuclear data. The resonance average data are represented by filled squares.

Fig.6 - $^{182}Ta$ strength function compared to the extrapolation of the photonuclear data.

Fig.7 - Cross sections for capture to the 2 $d_{5/2}$ doublet in $^{90}Y$. Comparison between CN and DSD predictions with the experimental data.

Fig.8 - Angle-integrated cross section for the γ-ray transition to the $g_{9/2}$ ground state of $^{209}Pb$.

Fig.9 - Energy dependence of the asymmetry factor in the $^{208}Pb(n,\gamma_o)$ reaction : E1 + E2 (dashed line), E1 + M1 (dotted line) and E1 + M1 + E2 (continuous line) excitations. Comparison with the measured values.

Fig.10 - Energy dependence of the asymmetry factor for the $\gamma_o$-transition in the $^{208}Pb(n,\gamma)$ reaction. Comparison between the predictions of the DSD model (continuous line) and the experimental data.

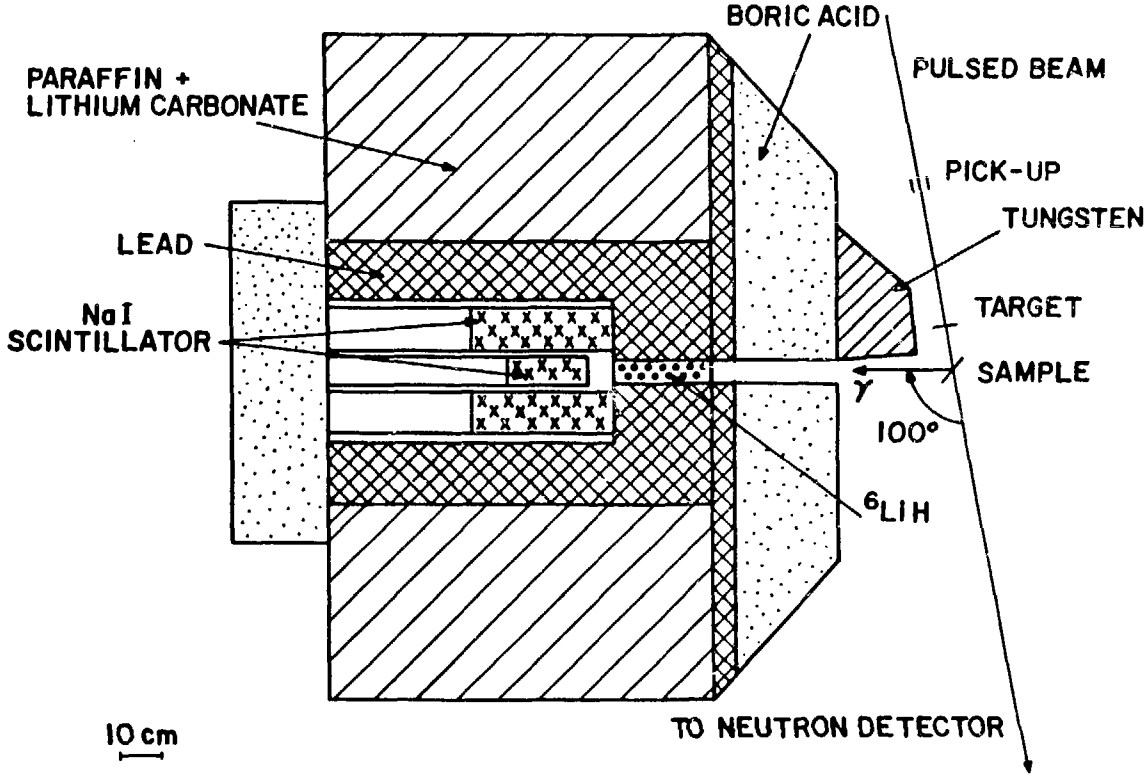
BORIC ACID
PULSED BEAM
PARAFFIN +
LITHIUM CARBONATE
PICK-UP
TUNGSTEN
LEAD
NaI
SCINTILLATOR
TARGET
SAMPLE
γ
100°
$^6$LiH
10 cm
TO NEUTRON DETECTOR

Figure 1

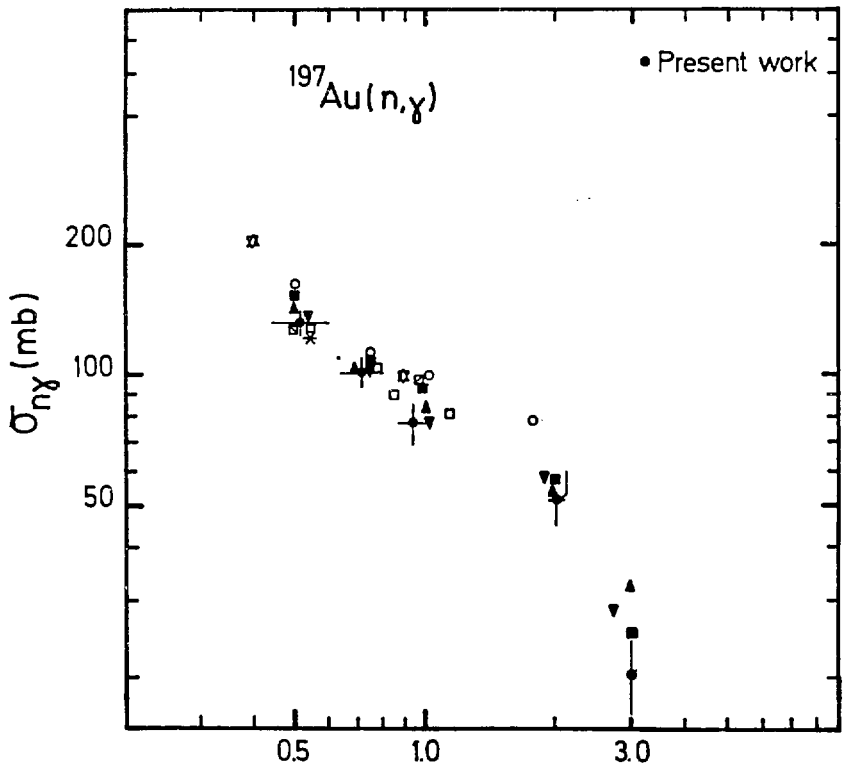


Figure 2

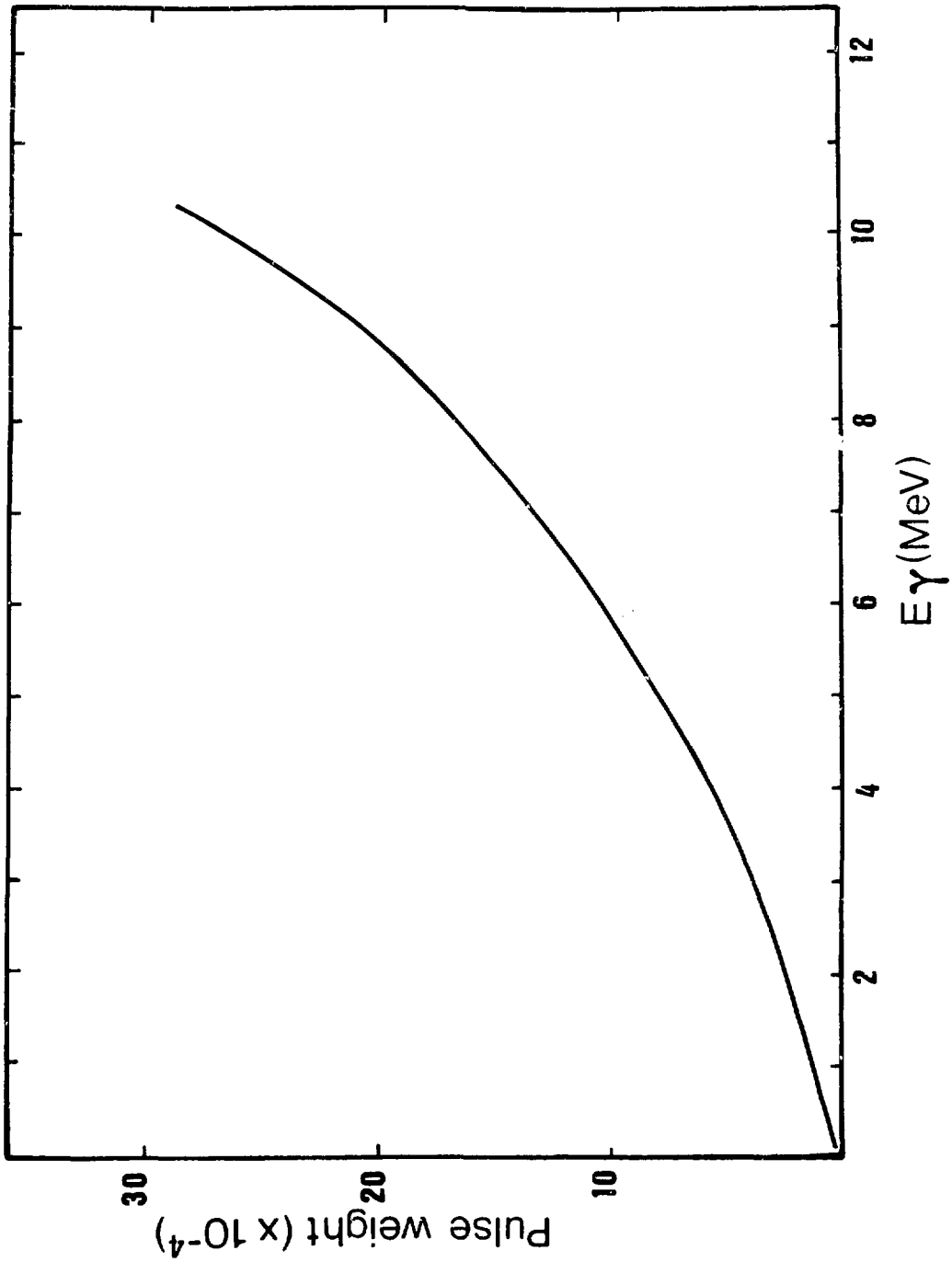


Figure 3

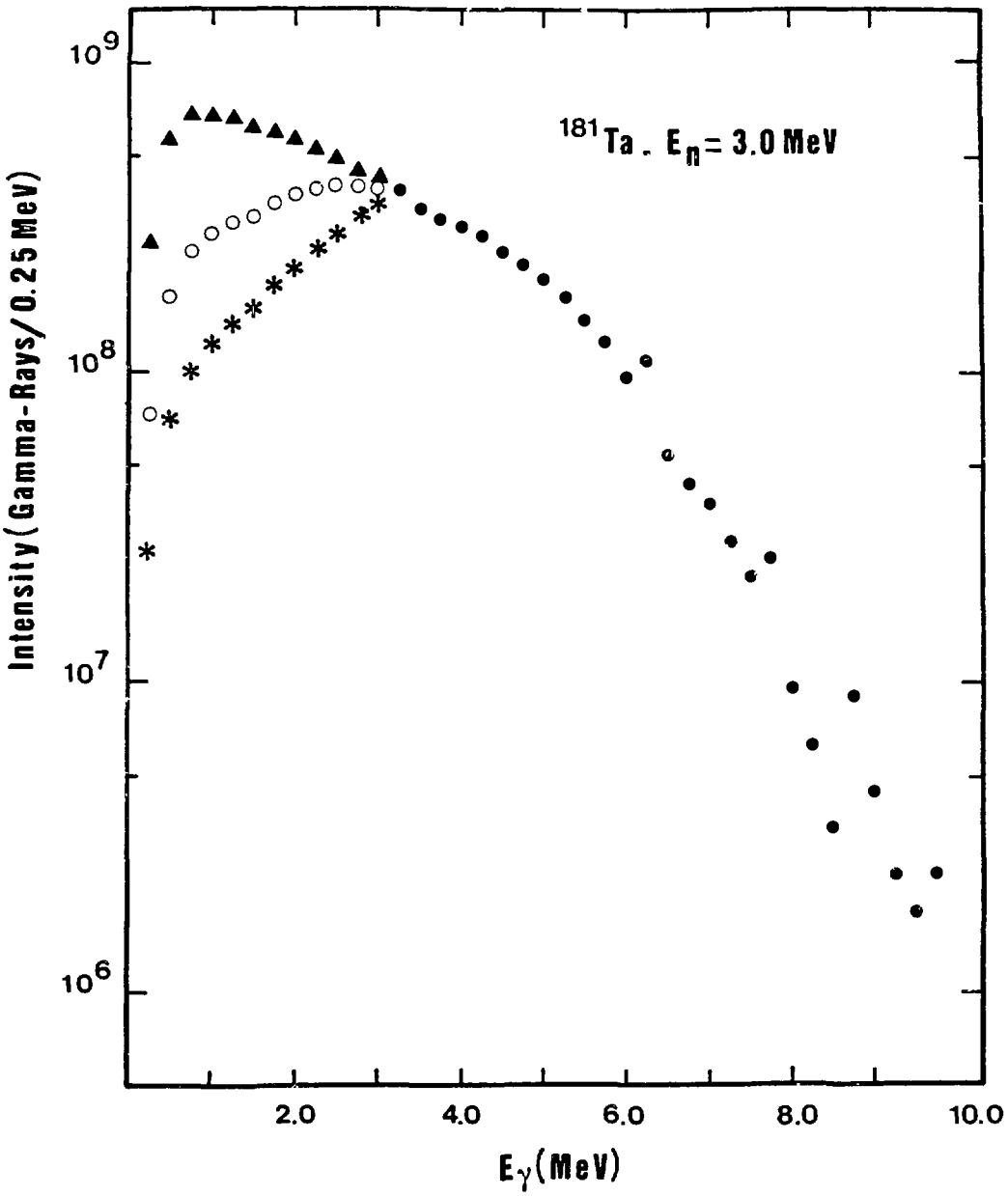
$^{181}$Ta . $E_n$ = 3.0 MeV
Intensity (Gamma-Rays/0.25 MeV)
$10^9$
$10^8$
$10^7$
$10^6$
2.0
4.0
6.0
8.0
10.0
$E_\gamma$ (MeV)

Figure 4

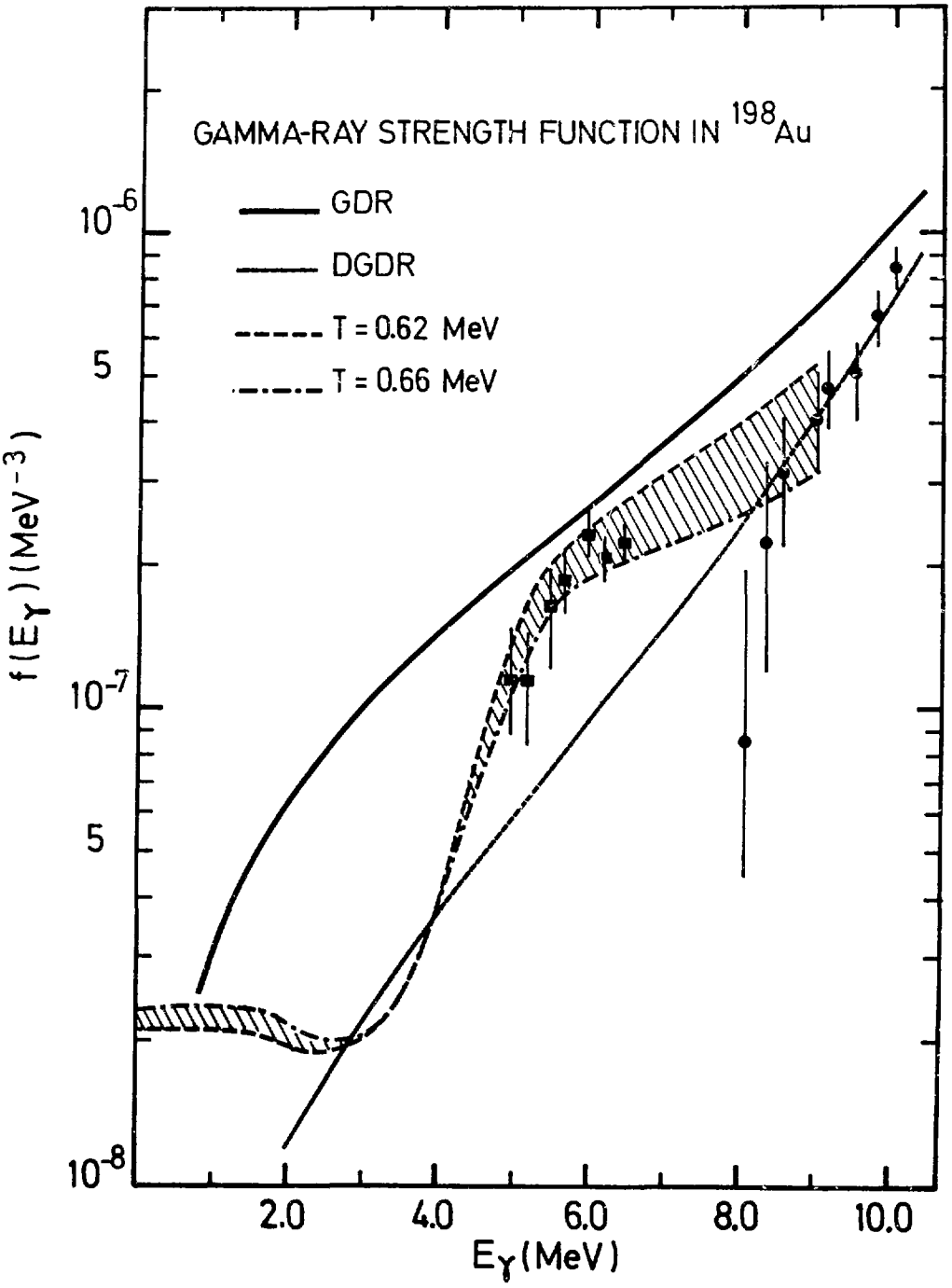
GAMMA-RAY STRENGTH FUNCTION IN 198Au
GDR
DGDR
T = 0.62 MeV
T = 0.66 MeV
f(Eγ) (MeV-3)
10-6
5
10-7
5
10-8
2.0
4.0
6.0
8.0
10.0
Eγ (MeV)

Figure 5

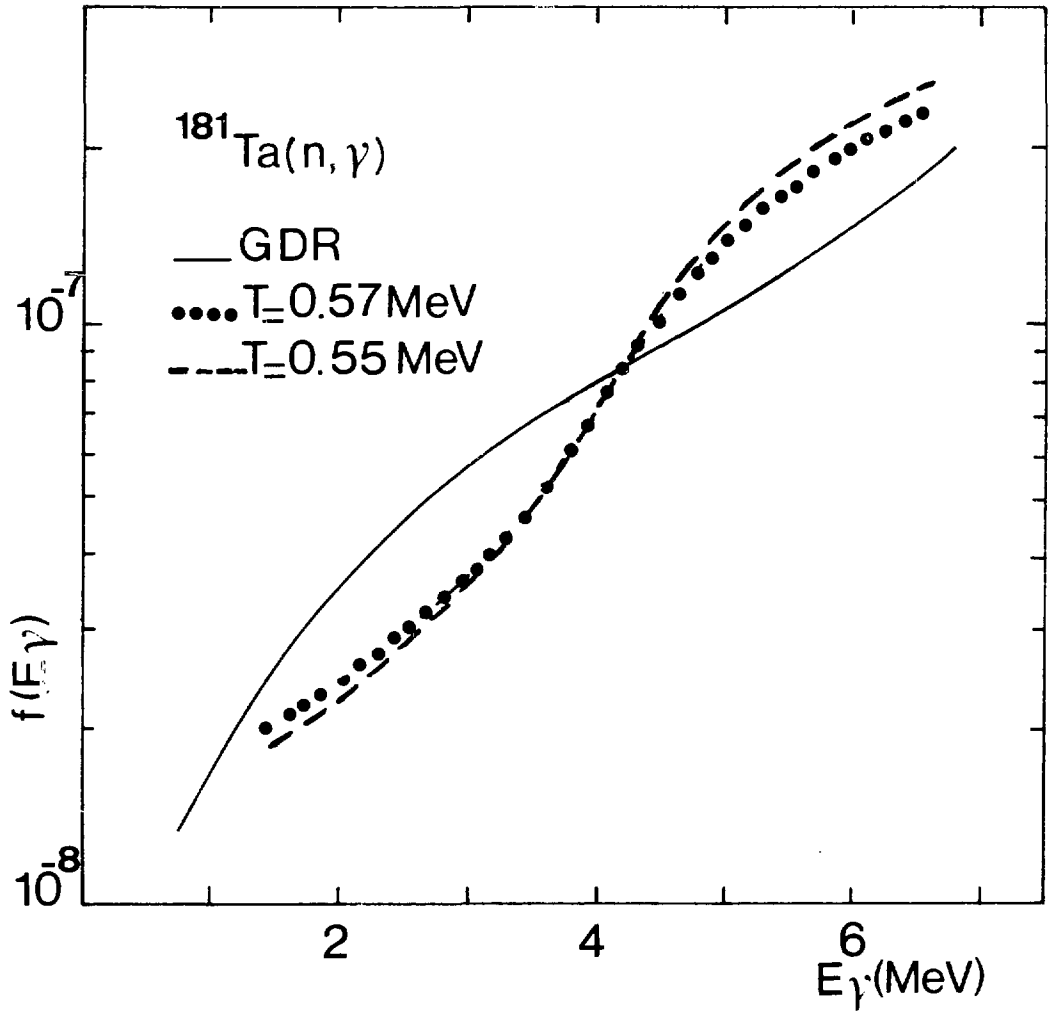


Figure 6

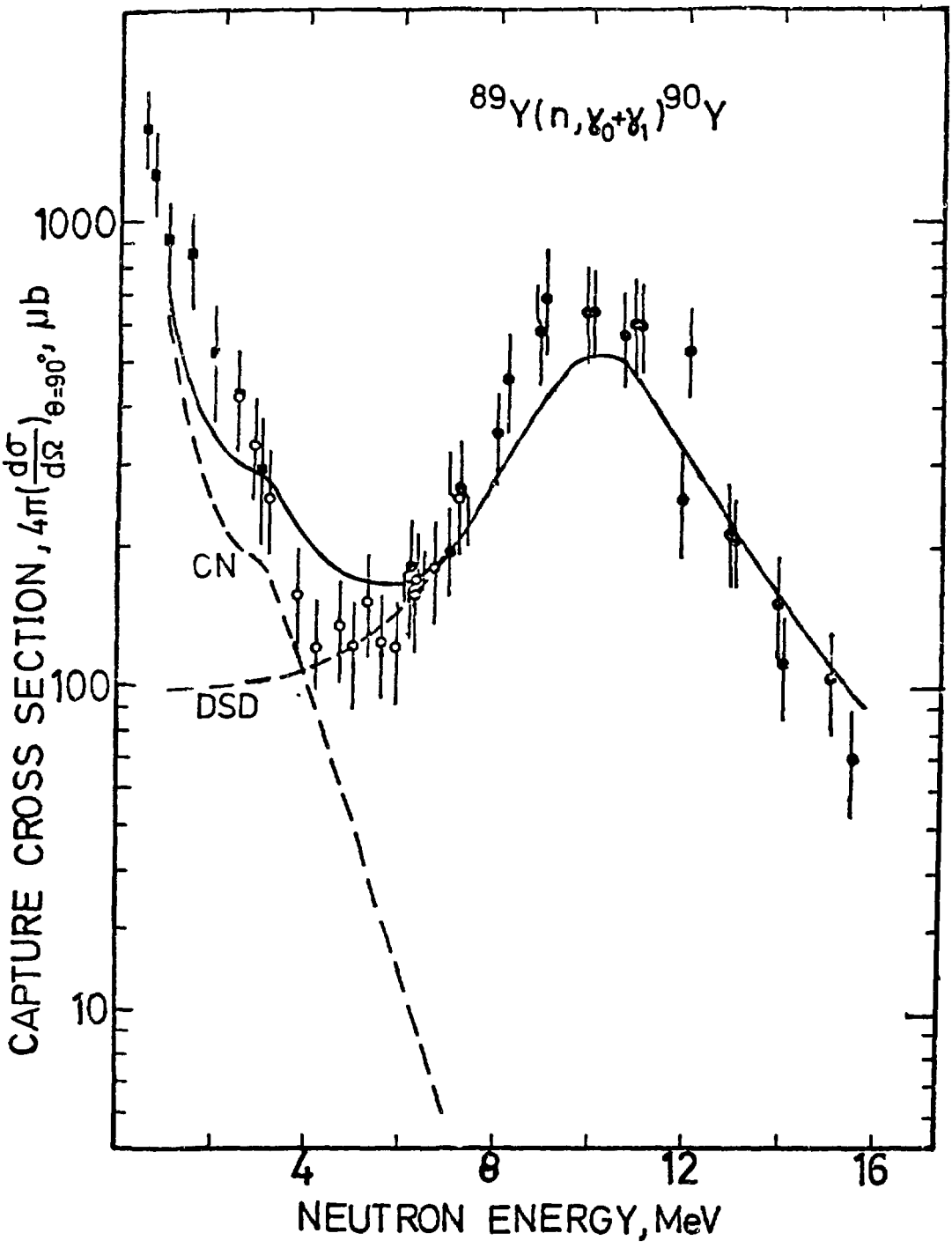
$^{89}Y(n,\gamma_0+\gamma_1)^{90}Y$
CAPTURE CROSS SECTION, $4\pi(\frac{d\sigma}{d\Omega})_{\theta=90°}$, μb
1000
100
10
CN
DSD
4
8
12
16
NEUTRON ENERGY, MeV

Figure 7

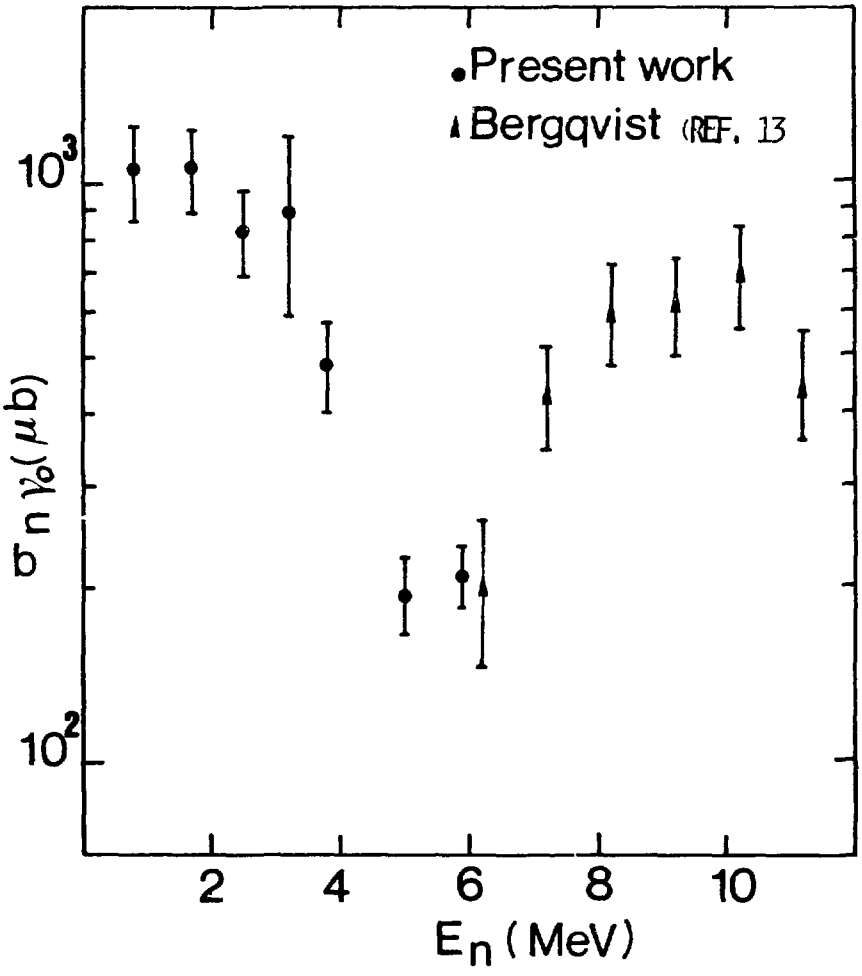
•Present work
▲Bergqvist (REF. 13
$10^3$
$10^2$
$\sigma_{n\gamma_0}(\mu b)$
2
4
6
8
10
$E_n$ (MeV)

Figure 8

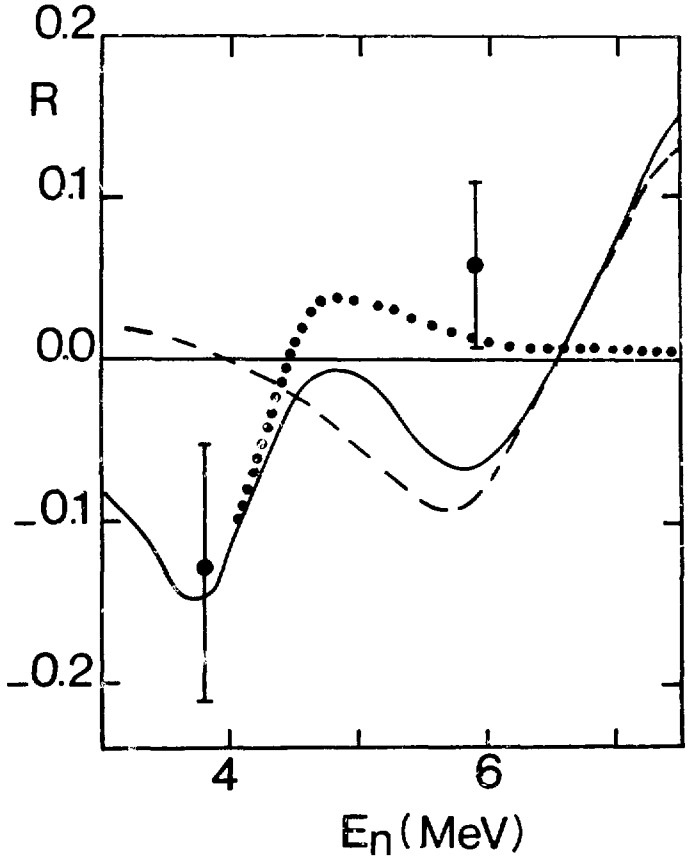


Figure 9

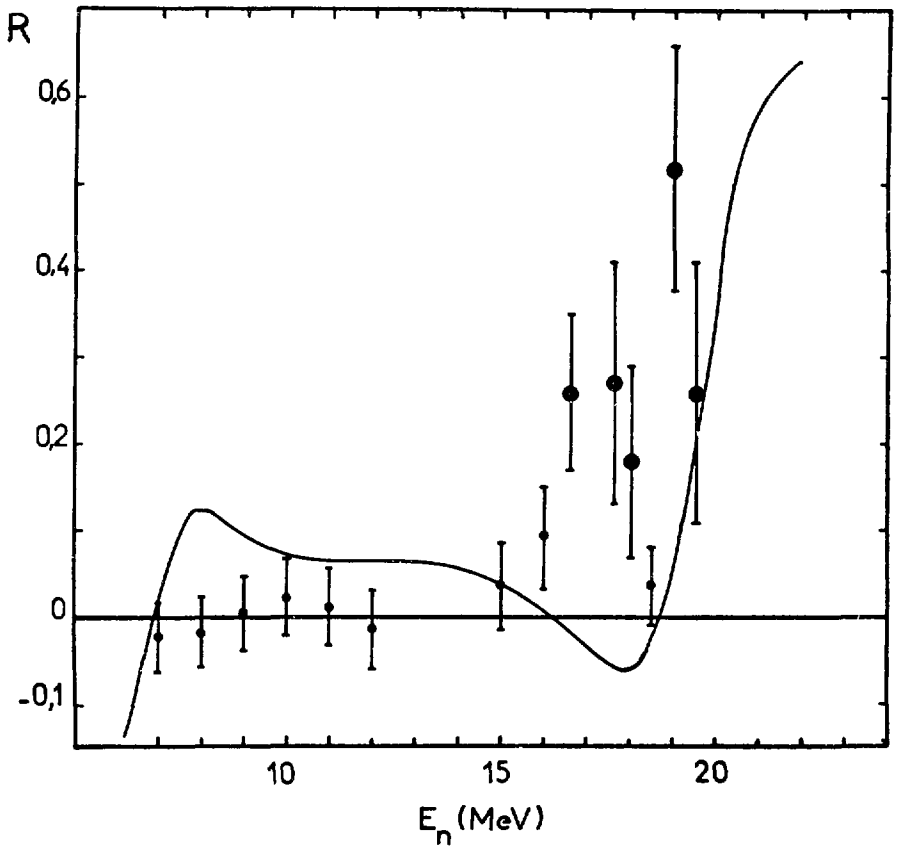


Figure 10

*Edité par*
*le Service de Documentation*
*Centre d'Etudes Nucléaires de Saclay*
*91191 GIF-sur-YVETTE Cédex (France)*